VALERI PROJECT
Website: http://www.avignon.inra.fr/valeri
CAMPAIGN 2002

GROUND DATA PROCESSING & PRODUCTION OF THE LEVEL 1 HIGH RESOLUTION MAPS

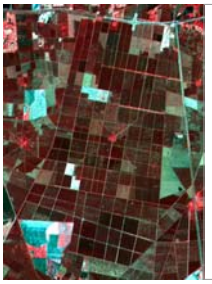

VALERI 2002

Nezer site
(pine forest)

Philippe Rossello

September 2006

CONTENTS

1. Introduction

This report describes the production of the high resolution, level 1, biophysical variable maps for the Nezer site in 2002 (see campaign report for more details about the site and the ground measurement campaign: annex or http://www.avignon.inra.fr/valeri). Level 1 map corresponds to the map derived from the determination of a transfer function between reflectance values of the SPOT image acquired during (or around) the ground campaign, and biophysical variable measurements (hemispherical images). For each Elementary Sampling Unit (ESU), the hemispherical images were processed using the CAN-EYE software (versions 3.2.4, 3.5.1 and 4.1) developed at INRA-CSE. The derived biophysical variable maps are:

• four Leaf Area Index (LAI) are considered: effective LAI (LAIeff) and true LAI (LAItrue) derived from the description of the gap fraction as a function of the view zenith angle; effective LAI57 (LAI57eff) and true LAI57 (LAI57true) derived from the gap fraction at 57.5°, which is independent on the leaf inclination. Effective LAI and effective LAI57 do not take into account clumping effect. LAItrue and LAI57true are derived using the method proposed by Lang and Yueqin[1] (1986);

• cover fraction (fCover): it is the percentage of soil covered by vegetation. To improve the spatial sampling, fCover was computed over 0 to 10° zenith angle;

• fAPAR: it is the fraction of Absorbed Photosynthetically Active Radiation (PAR=400-700nm). The fAPAR is defined either instantaneously (for a given solar position) or integrated all over the day. Following a study based on radiative transfer model simulations, it has been shown that the root mean square error between instantaneous fAPAR computed every 30 minutes and the daily fAPAR is the lowest for instantaneous fAPAR at 10h00 AM (solar time, RMSE = 0.021). Therefore, the derivation of fAPAR from CAN-EYE corresponds to the instantaneous black sky fAPAR at 10h00 AM.

The land cover is mainly composed of maritime pines (forest). The site is “nearly flat” (for more information, see annex or campaign report: http://www.avignon.inra.fr/valeri).

The site coordinates are described in Table 1:

	France Zone III sud, Nouvelle Triangulation Française IGN (units = meters)		Geographic Lat/Lon, WGS-84 (units = degrees)		UTM 30 North, WGS-84 (units = meters)	
	Easting	Northing	Lat.	Lon.	Easting	Northing
Upper left corner	327992.4000	263018.1000	44.61617329	-1.09170756	651403.8179	4942084.7363
Lower right corner	336032.4000	251978.1000	44.51986535	-0.98487525	660144.0833	4931590.7571
Center	332012.4000	257498.1000	44.56803208	-1.0382477	655773.9375	4936837.8411

Table 1. Description of the site coordinates: they correspond to SPOT image coordinates.

2. Available data

2.1. SPOT Image

The SPOT image was acquired the 21th April 2002 by HRVIR2 on SPOT4 while the ground measurements were carried out the 23/04/2002. The initial projection is France Zone III sud, Nouvelle Triangulation Française IGN (please, refer to the campaign report for more details: annex or http://www.avignon.inra.fr/valeri). The image was geo-located by SPOT image (SPOTViewBasic product, precision 2B). No atmospheric correction was applied to the image. However, as the SPOT image is used to compute empirical relationships between reflectance and biophysical variable, we can assume that the effect of the atmosphere is the same over the whole 8 x 11 km site. Therefore, it will be taken into account everywhere in the same way.

Figure 1 shows the relationship between Red and near infrared (NIR) SPOT channels: the soil line is well marked and no saturated points are observed.

[1] Lang, A.R.G. and Yueqin, X., 1986. Estimation of leaf area index from transmission of direct sunlight in discontinuous canopies. Agric. For. Meteorol., 37: 229-243.

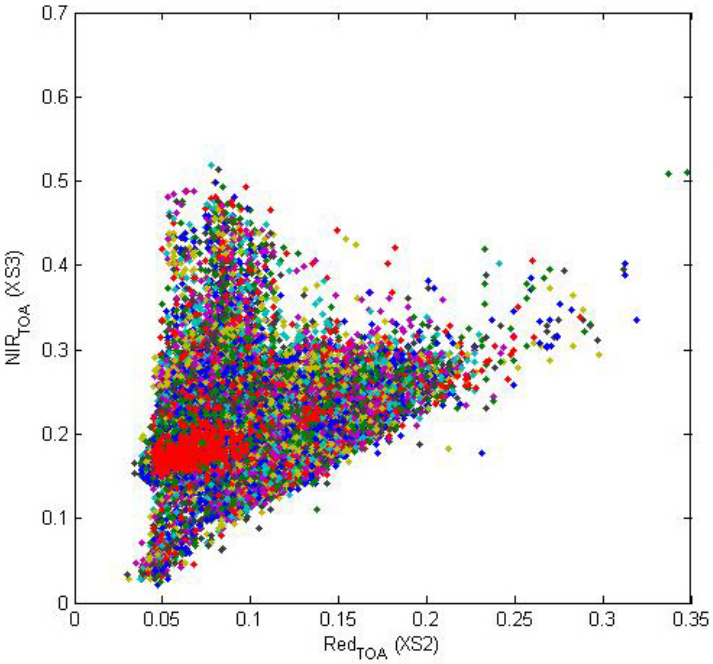

Figure 1. Red/NIR relationship on the SPOT image for Nezer, 2002.

2.2. Hemispherical images

The hemispherical images were processed using the CAN-EYE software (versions 3.2.4, 3.5.1 and 4.1) to derive the biophysical variables. Note that the version 4.1 was used to estimate the "green vegetation".

Figure 2 and Figure 3 show the distribution of the several variables over the 68 sampled ESUs. As there was understorey on six ESUs (E632, E632T1, E632T6, E632T7, E671 and E1042), hemispherical images were acquired from above the understorey and from below the canopy (trees). The two sets of acquisition were processed separately to derived LAI (effective and true), LAI57 (effective and true), fCover, and fAPAR. The ESU biophysical variable was then computed as:

- LAIeff, LAI57eff, LAItrue, LAI57true: LAI(above) + LAI(below).
- fCover: 1-(1-fCover(above))*(1-fCover(below)). This assumes that independency of the gaps inside the understorey and the gaps inside the trees which is not true at all the scales but it is the only way to get the total fCover. However, for the local scales considered, this might be true as a first order approximation.
- fAPAR: [1-(1-fAPAR(below))*(1-fAPAR(above))], since 1-fAPAR can be considered equivalent to a gap fraction. Here again, the same independency between the two layers has to be assumed.

Note that LAI (effective and true) derived from directional gap fraction and LAI derived from gap fraction at 57.5° (effective and true) are consistent (Figure 2 and Figure 3). Effective LAI (LAIeff, LAI57eff) varies from 0 to 3.03, while true LAI (LAItrue, LAI57true) varies from 0 to 5.13. This range shows a heterogeneous site in terms of LAI. For values, LAIeff and LAI57eff are lower than LAItrue and LAI57true. This is due to the clumping observed for several ESUs. The relationship between fAPAR and LAI is in agreement with what is expected (Beer-Lambert law) while the fCover-LAI relationship is more noisy.

To build the relationships between biophysical variables and SPOT data, the reflectance of a given forest ESU was considered as the average reflectance over the central pixel + the 8 surrounding pixels. This takes into account the fact that the height of the trees are about 18 m and consequently the fish-eye observes an area of $\pi \times [18 \times \tan(60°)]^2 \cong 3050$ m², *i.e.* close to the area of 9 SPOT pixels (=3600m²) when using a maximum view zenith angle of 60°.

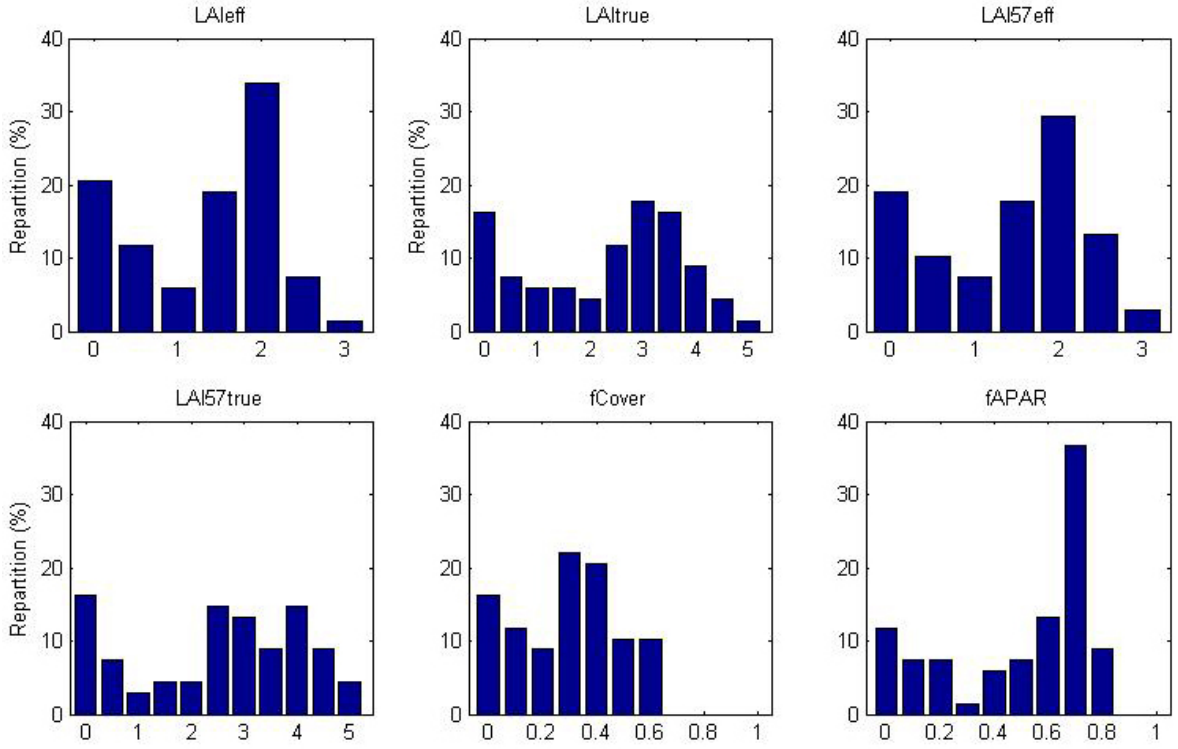

Figure 2. Distribution of the measured biophysical variables over the ESUs.

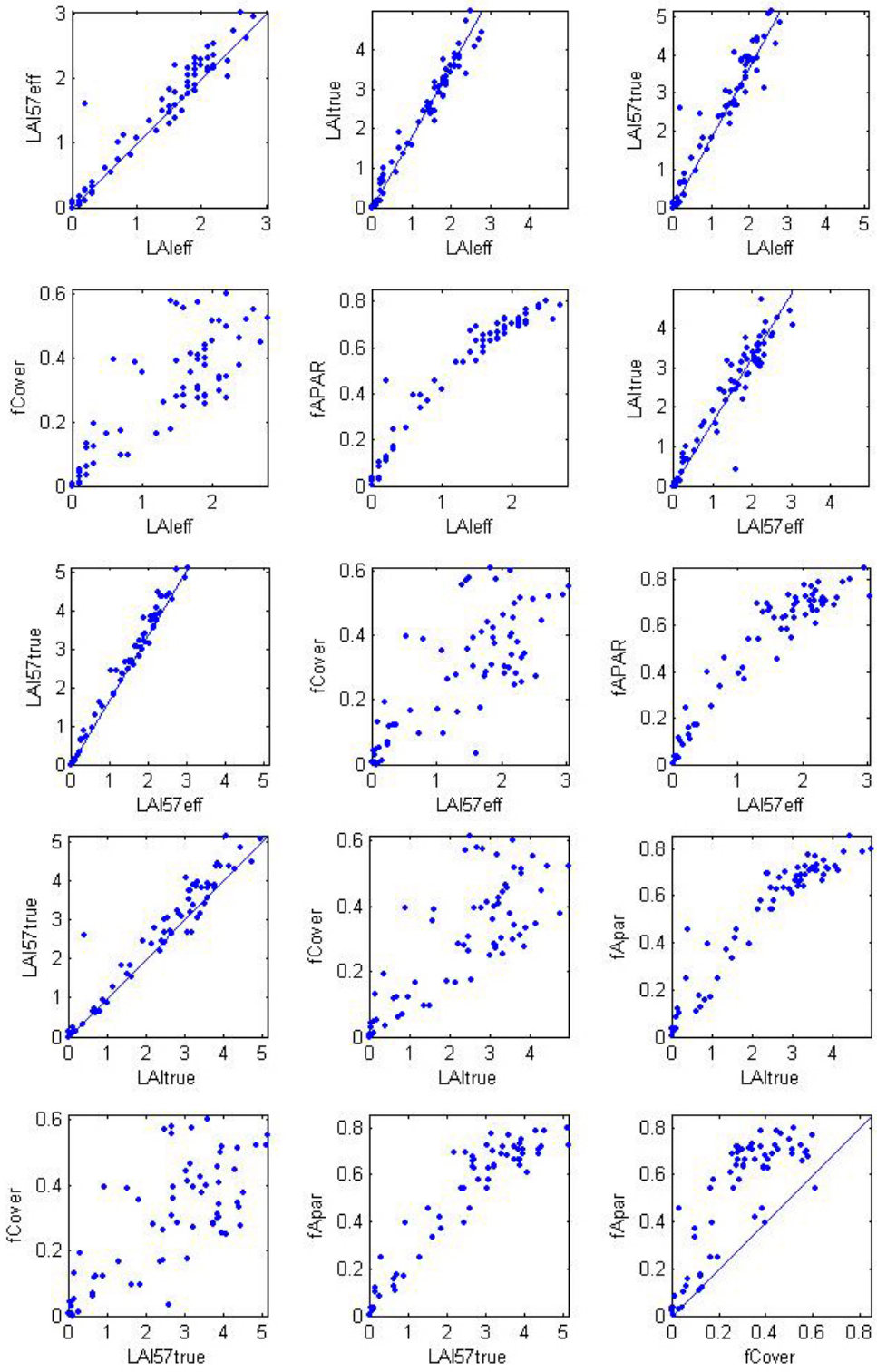

Figure 3. Relationships between the different biophysical variables

2.3. Sampling strategy

2.3.1. Principles

The sampling strategy is defined in the campaign report: http://www.avignon.inra.fr/valeri. Figure 4 shows that the 68 ESUs are evenly distributed over the site (8 x 11 km), even if the experiment in 2002 was focused in the central part of the study area.

The processing of the ground data has shown that:

• considering that SPOT geo-location and GPS measurements are associated to errors, we found that processed LAI for ESUs E632T5, E632T9, E1141 and E1392T1 did not correspond to the SPOT pixels in terms of reflectance as compared to the knowledge of the land use: it has been shifted by 1 or 2 pixels.

Finally, the 68 ESUs have been kept for the computation of the transfer function.

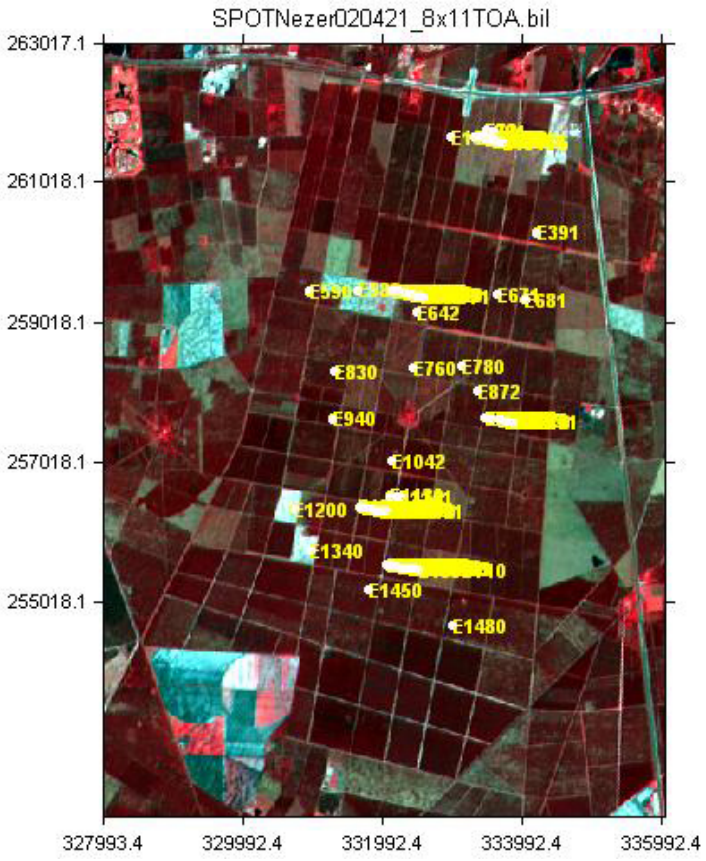

Figure 4. Distribution of the ESUs around the Nezer site.

2.3.2. Evaluation based on NDVI values

The sampling strategy is evaluated using the SPOT image by comparing the NDVI distribution over the site with the NDVI distribution over the ESUs (Figure 5). As the number of pixels is drastically different for the ESU and whole site (WS = 220000 in case of a 8 x 11 km SPOT image at 20 m resolution), it is not statistically consistent to directly compare the two NDVI histograms. Therefore, the proposed technique consists in comparing the NDVI cumulative frequency of the two distributions by a Monte-Carlo procedure which aims at comparing the actual frequency to randomly shifted sampling patterns. It consists in:

1. computing the cumulative frequency of the *N* pixel NDVI that correspond to the exact ESU locations;
2. then, applying a unique random translation to the sampling design (modulo the size of the image);
3. computing the cumulative frequency of NDVI on the randomly shifted sampling design;
4. repeating steps 2 and 3, 199 times with 199 different random translation vectors.

This provides a total population of $N = 199 + 1$(actual) cumulative frequency on which a statistical test at acceptance probability $1 - \alpha = 95\%$ is applied: for a given NDVI level, if the actual ESU density function is between two limits defined by the $N\alpha/2 = 5$ highest and lowest values of the 200 cumulative frequencies, the hypothesis assuming that WS and ESU NDVI distributions are equivalent is accepted, otherwise it is rejected.

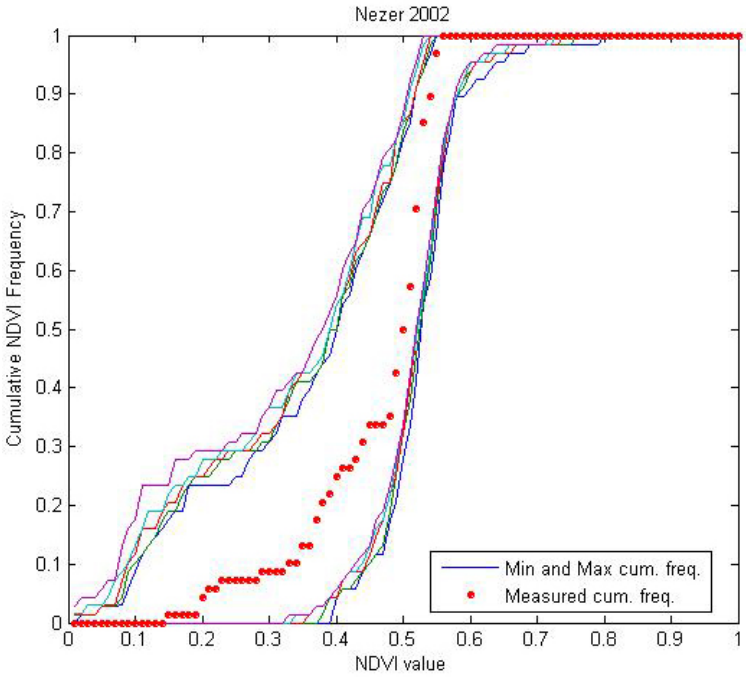

Figure 5. Comparison of the ESU NDVI distribution and the NDVI distribution over the whole image.

Figure 5 shows that the NDVI distribution of the 68 ESUs is very good as compared to the NDVI distribution over the whole site since the 'ESU' curve is inside the 'boundary curves'. Note that NDVIs lower than 0.15 (bare soil, roads, paths…) and higher than 0.56 have not been sampled although they are present in the image. The sampling of NDVI values between 0.23 and 0.32 appears also insufficient, even if the NDVI distribution is very satisfactory.

2.3.3. Evaluation based on classification

A non supervised classification based on the k_means method (Matlab statistics toolbox) was applied to the reflectance of the SPOT image to distinguish if different behaviours on the image for the biophysical variable-reflectance relationship exist.

A number of 5 classes was chosen (Figure 6). The distribution of the classes on the image and on the ESUs is rather similar: classes 1, 3 and 4 are under-represented while classes 2 and 6 appear to be over-sampled.

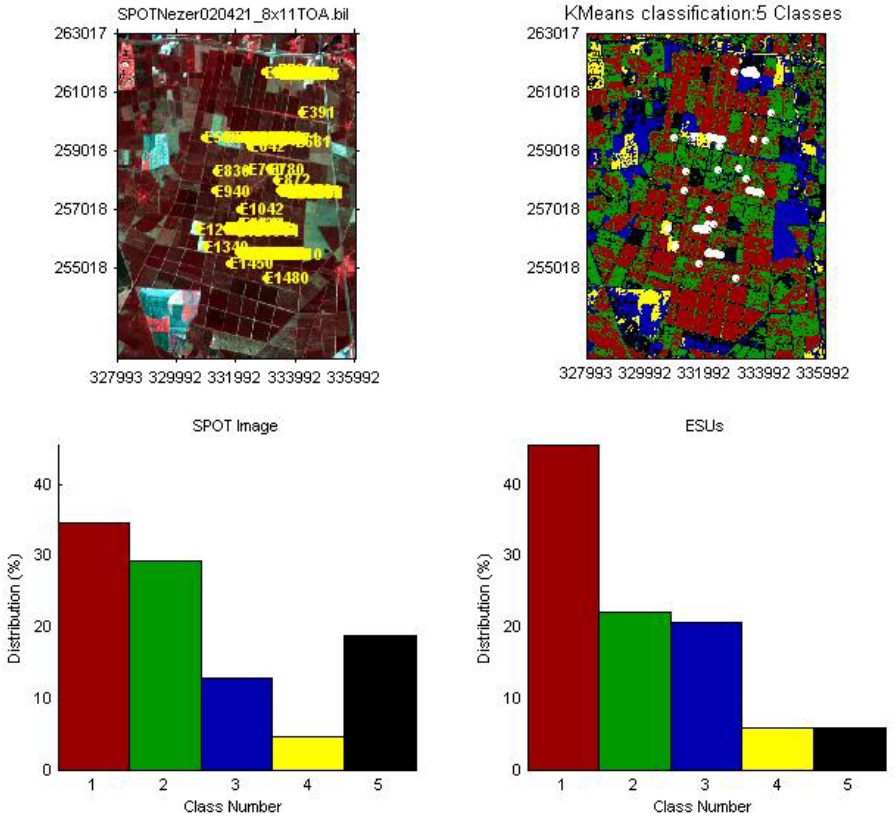

Figure 6. Classification of the SPOT image. Comparison of the class distribution between the SPOT image and sampled ESUs.

Figure 7 shows the different relationships observed between the biophysical variables and the corresponding NDVI on the ESUs, as a function of the SPOT classes determined from non supervised classification.

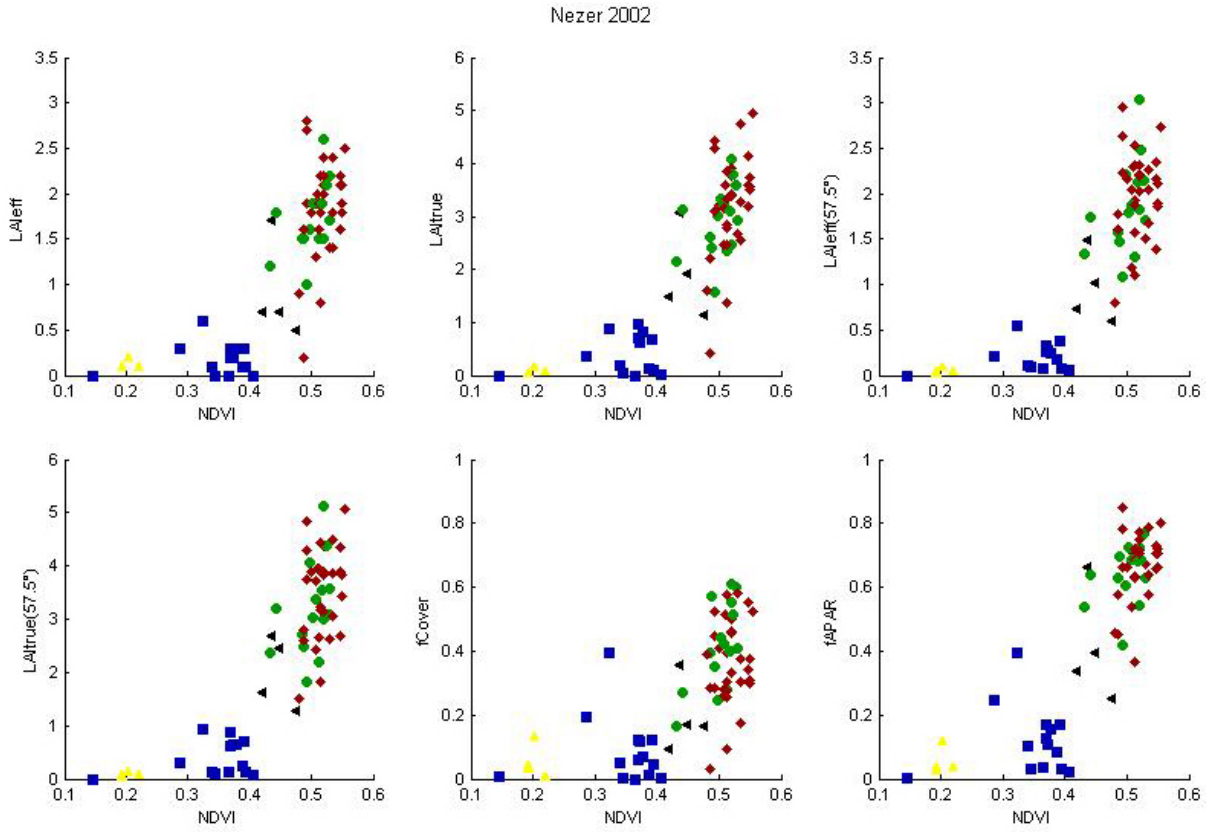

Figure 7. NDVI-Biophysical Variable relationships as a function of SPOT classes

Even if no different behaviour between the classes can be observed, note that the class 3 is distinguishable from others classes: several NDVI values are relatively high while biophysical variable values (E181T5, E191, E191T1, E191T3, E191T5, E632T8) are low or null. The pixels correspond to "young pine stand" or "clear cut" (please, refer to the campaign report for more details: annex or http://www.avignon.inra.fr/valeri). However, a single transfer functions will be generated.

2.3.4. Using convex hulls

A test based on the convex hulls was also carried out to characterize the representativeness of ESUs. Whereas the evaluation based on NDVI values uses two bands (red and NIR), this test uses the four bands of the SPOT image. A flag image, is computing over the reflectances (Figure 8). The result on convex-hulls can be interpreted as:

- pixels inside the 'strict convex-hull': a convex-hull is computed using all the SPOT reflectance corresponding to the ESUs belonging to the class. These pixels are well represented by the ground sampling and therefore, when applying a transfer function the degree of confidence in the results will be quite high, since the transfer function will be used as an interpolator;
- pixels inside the 'large convex-hull': a convex-hull is computed using all the reflectance combination (±5% in relative value) corresponding to the ESUs. For these pixels, the degree of confidence in the obtained results will be quite good, since the transfer function is used as an extrapolator (but not far from interpolator);
- pixels outside the two convex-hulls: this means that for these pixels, the transfer function will behave as an extrapolator which makes the results less reliable. However, having a priori information on the site may help to evaluate the extrapolation capacities of the transfer function.

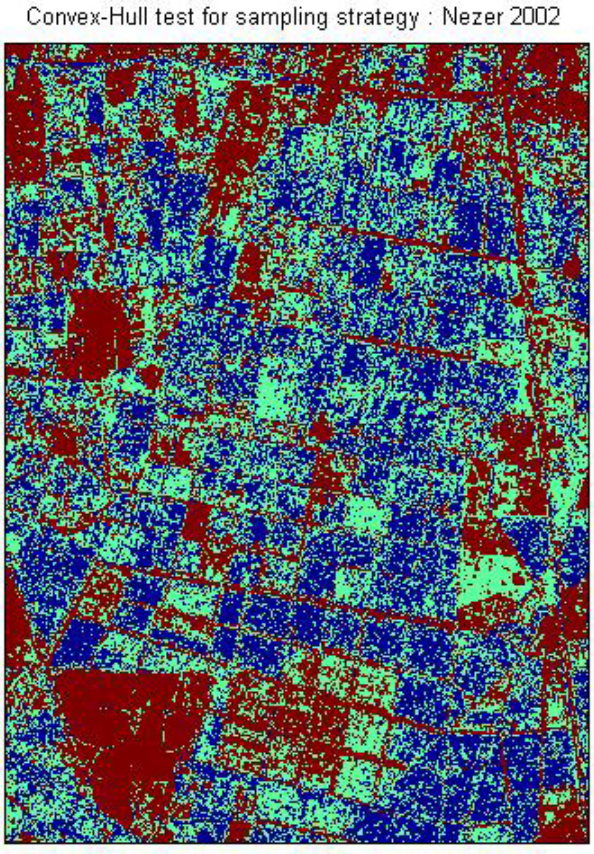

Figure 8. Evaluation of the sampling based on the convex hulls. The map is shown at the bottom: blue and light blue correspond to the pixels belonging to the 'strict' and 'large' convex hulls and red to the pixels for which the transfer function is extrapolating.

This map shows that the representativeness of the ESUs is satisfactory, even if pixels are outside the two convex-hulls. They mainly correspond to bare soil, roads, paths, but also highest NVDI pixels and a few intermediate NDVI values (§2.3.2).

3. Determination of the transfer function for the 6 biophysical variables: LAIeff, LAI57eff, LAItrue, LAI57true, fCover, fAPAR

3.1. The transfer function considered

For each class determined in §2.3, a single transfer function was tested:

- REG: if the number of ESUs is sufficient, multiple robust regression between ESUs reflectance (or Simple Ratio) and the considered biophysical variable can be applied: we used the 'robustfit' function from the Matlab statistics toolbox. It uses an iteratively re-weighted least squares algorithm, with the weights at each iteration computed by applying the bisquare function to the residuals from the previous iteration. This algorithm provides lower weight to ESUs that do not fit well. The results are less sensitive to outliers in the data as compared with ordinary least squares regression. At the end of the processing, three errors are computed: classical root mean square error (RMSE), weighted RMSE (using the weights attributed to each ESU) and cross-validation RMSE (leave-one-out method).

For the classes 1, 2, 3, 4 and 5, the 'REG' function is tested using either the reflectance or the logarithm of the reflectance for any band combination as well as the simple ratio or NDVI. As the method has poor extrapolation capacities, a flag image, based on the convex hulls is computing over reflectances.

3.2. Results

3.2.1. Choice of the method

For all the ESUs, a single transfer function was computed. Figure 9 shows the results obtained for all the possible band combinations using either the reflectance (ρ) or the logarithm of the reflectance (log(ρ)). Even if the regression made on the log(ρ) provides slightly better results (LAI variables and fAPAR), the results using the reflectance (ρ) were selected. For LAI variables, the transfer function using the log(ρ) creates coplanar points which do not allow the determination of the 'strict' and 'large' convex hulls. For fAPAR, the transfer function using the log(ρ) provides negative LAI values: even if these values are put to 0, the biophysical variable maps are not pertinent. For fCover, the results using the reflectance (ρ) were selected because they were better. Therefore, the results using the reflectance which are satisfactory were selected.

Note that the Red*NIR ('+' or RN) combination is added to all the band combinations (except for NDVI and SR). Please read the document: "a method to improve the relation between the biophysical variables" (http://www.avignon.inra.fr/valeri/table_methods/new_linear.pdf).

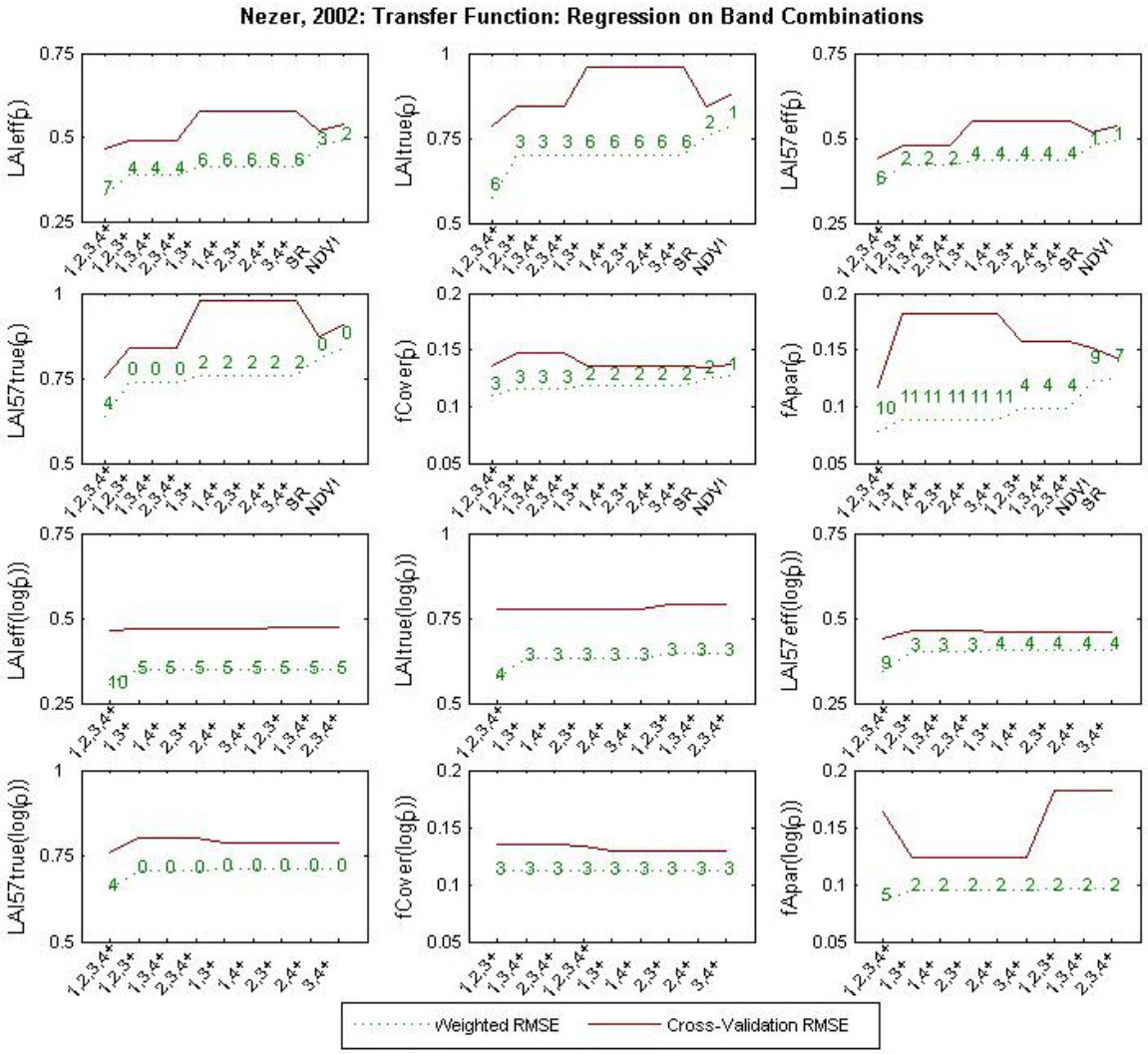

Figure 9. Transfer function: test of multiple regression applied on different band combinations. Band combinations are given in abscissa. The estimated biophysical variable is given in ordinate. Top graphs correspond to regression made on reflectance (ρ): the weighted root mean square error (RMSE) is presented in green along with the cross-validation RMSE in red. The numbers indicate the number of data used for the robust regression with a weight lower than 0.7 that could be considered as outliers. Bottom graphs correspond to regression made on the logarithm of the reflectance.

3.2.2. Choice of the band combination

For the LAIeff, the XS2, XS3, XS4, RN (Figure 10 and Figure 11) combination on reflectance was selected since it provides a good compromise between the cross-validation RMSE (among the lowest values), the weighted root mean square error (among the lowest values) and the number of weights lower than 0.7 (four). The following band combinations provide the same results: [XS1, XS2, XS3, RN]; [XS1, XS3, XS4, RN].

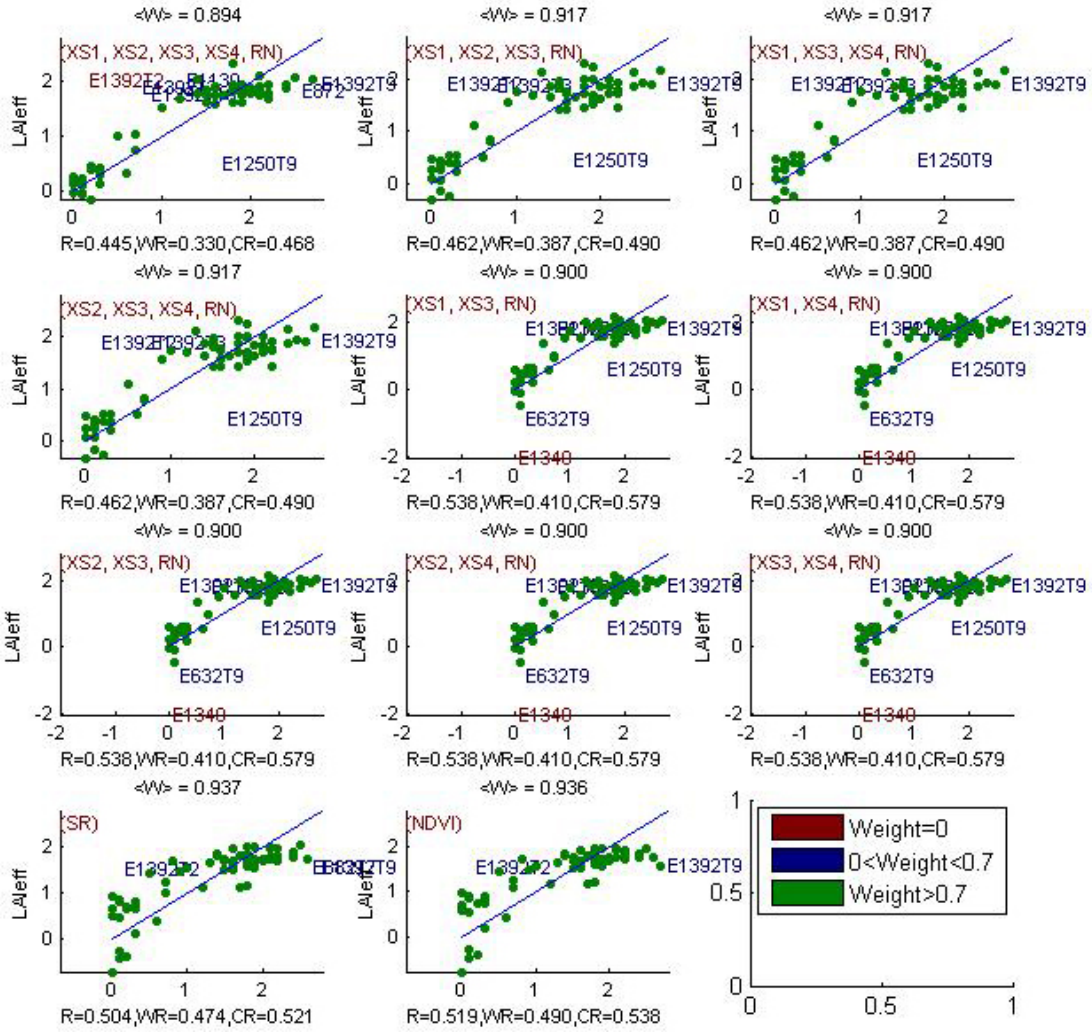

Figure 10. Effective Leaf Area Index: results for regression on reflectance using different band combinations. R is the root mean square error computed between LAIeff and estimated LAIeff. WR is the weighted root mean square error and CR is the cross validation root mean square error.

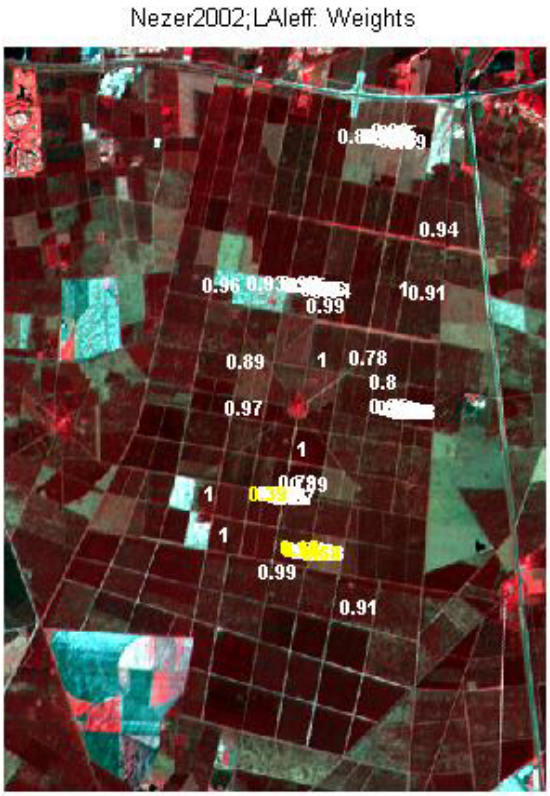

Figure 11. Weights associated to each ESU for the determination of LAIeff transfer function.

For the LAItrue, the XS1, XS2, XS3, XS4, RN (Figure 12 and Figure 13) combination on reflectance was selected since it provides the better results. Note that six weights are lower than 0.7.

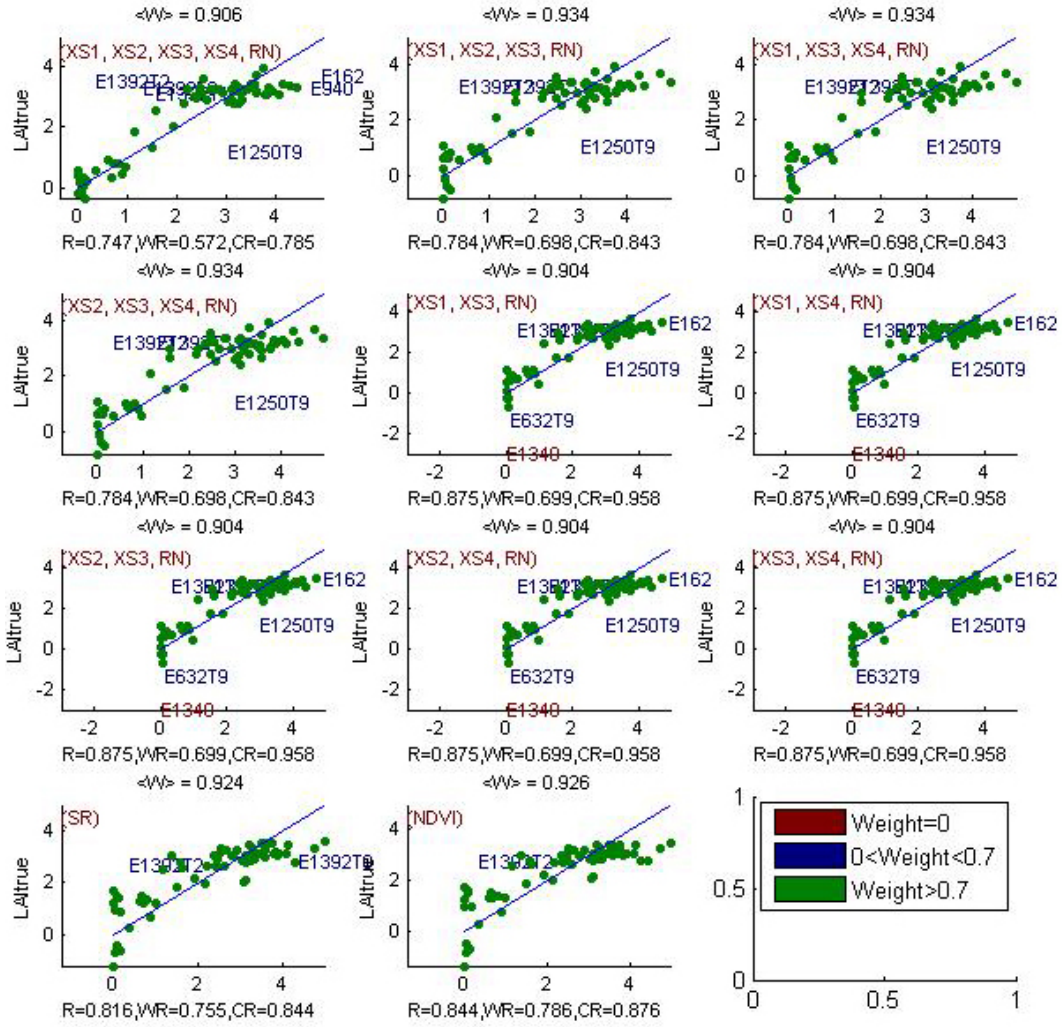

Figure 12. True Leaf Area Index: results for regression on reflectance using different band combinations. R is the root mean square error computed between LAItrue and estimated LAItrue. WR is the weighted root mean square error and CR is the cross validation root mean square error.

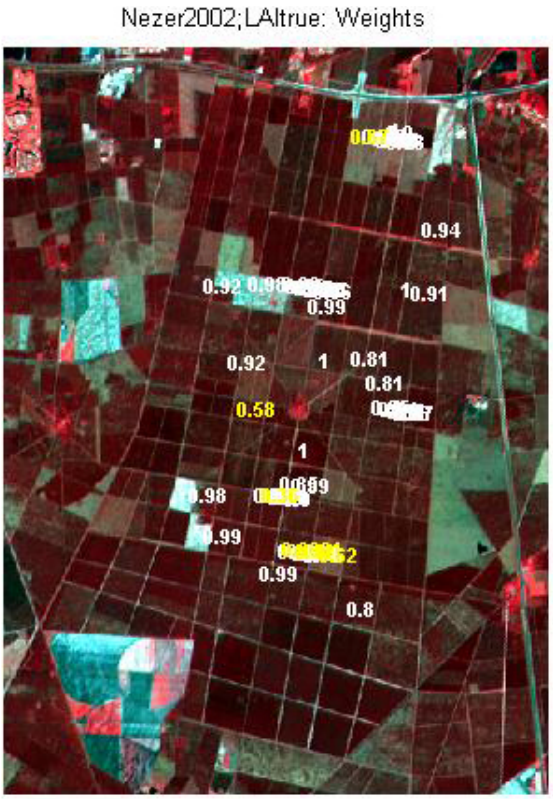

Figure 13. Weights associated to each ESU for the determination of LAItrue transfer function.

For the LAI57eff, the XS1, XS2, XS3, XS4, RN (Figure 14 and Figure 15) combination on reflectance was selected since it provides the better results: lowest R, CR and WR values. Note that six weights are lower than 0.7.

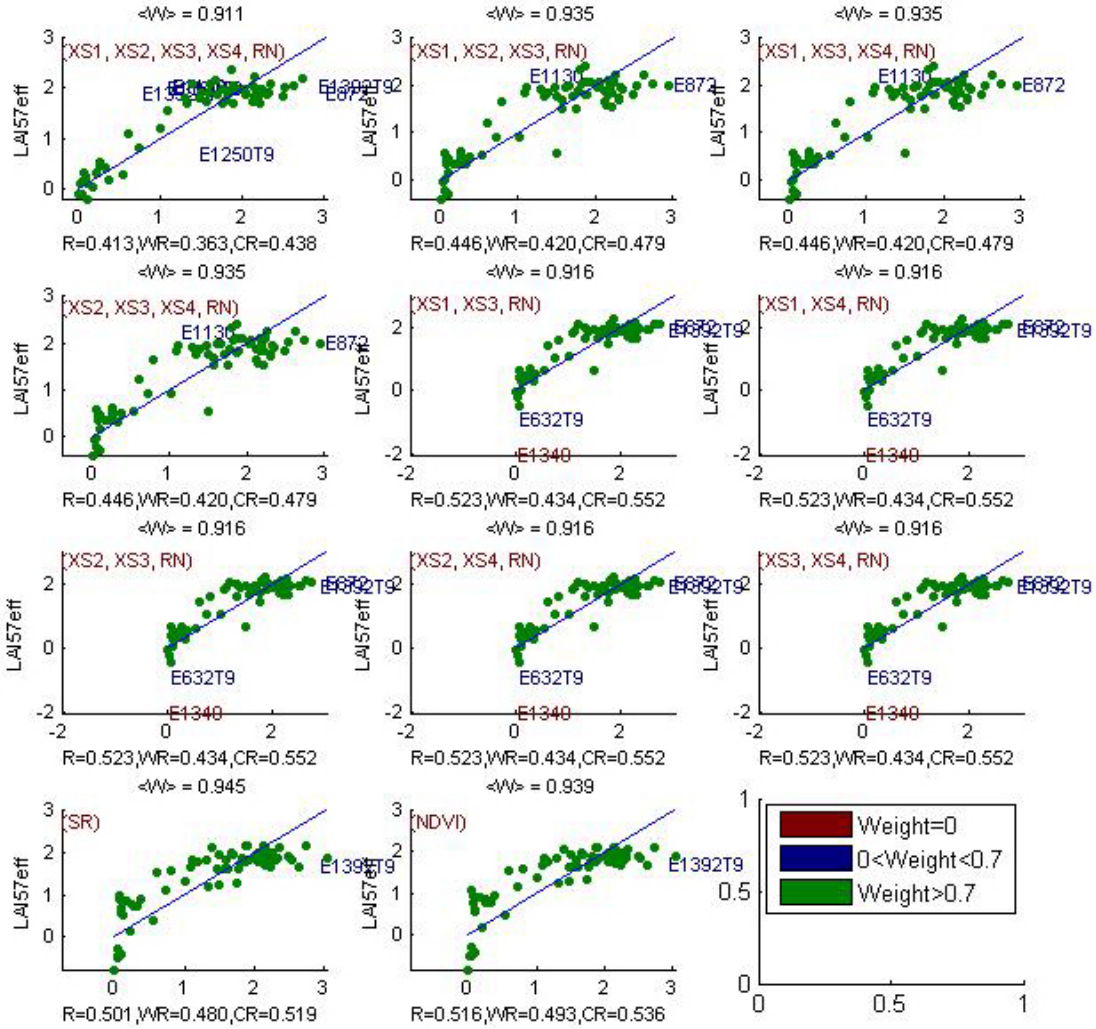

Figure 14. Effective LAI at 57.5°: results for regression on reflectance using different band combinations. R is the root mean square error computed between LAI57eff and estimated LAI57eff. WR is the weighted root mean square error and CR is the cross validation root mean square error.

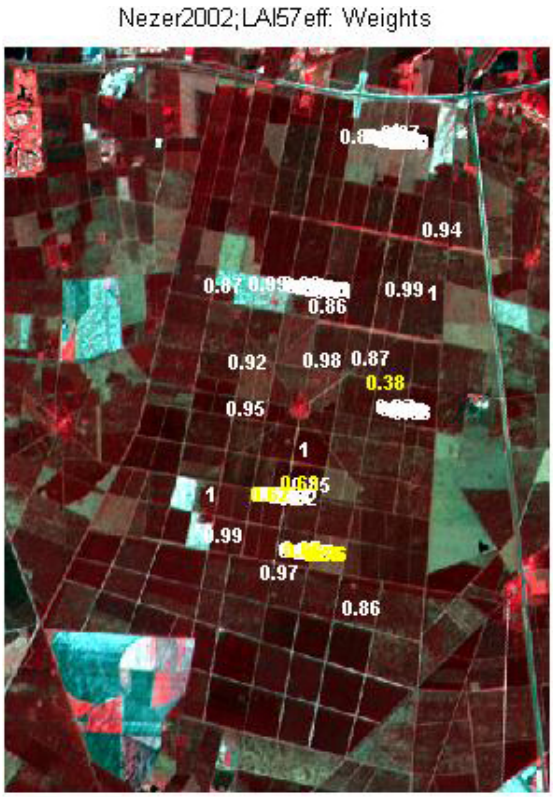

Figure 15. Weights associated to each ESU for the determination of LAI57eff transfer function.

For the LAI57true, the XS1, XS2, XS3, XS4, RN (Figure 16 and Figure 17) combination on reflectance was selected since it provides the better results: lowest R, CR and WR values. Note that four weights are lower than 0.7.

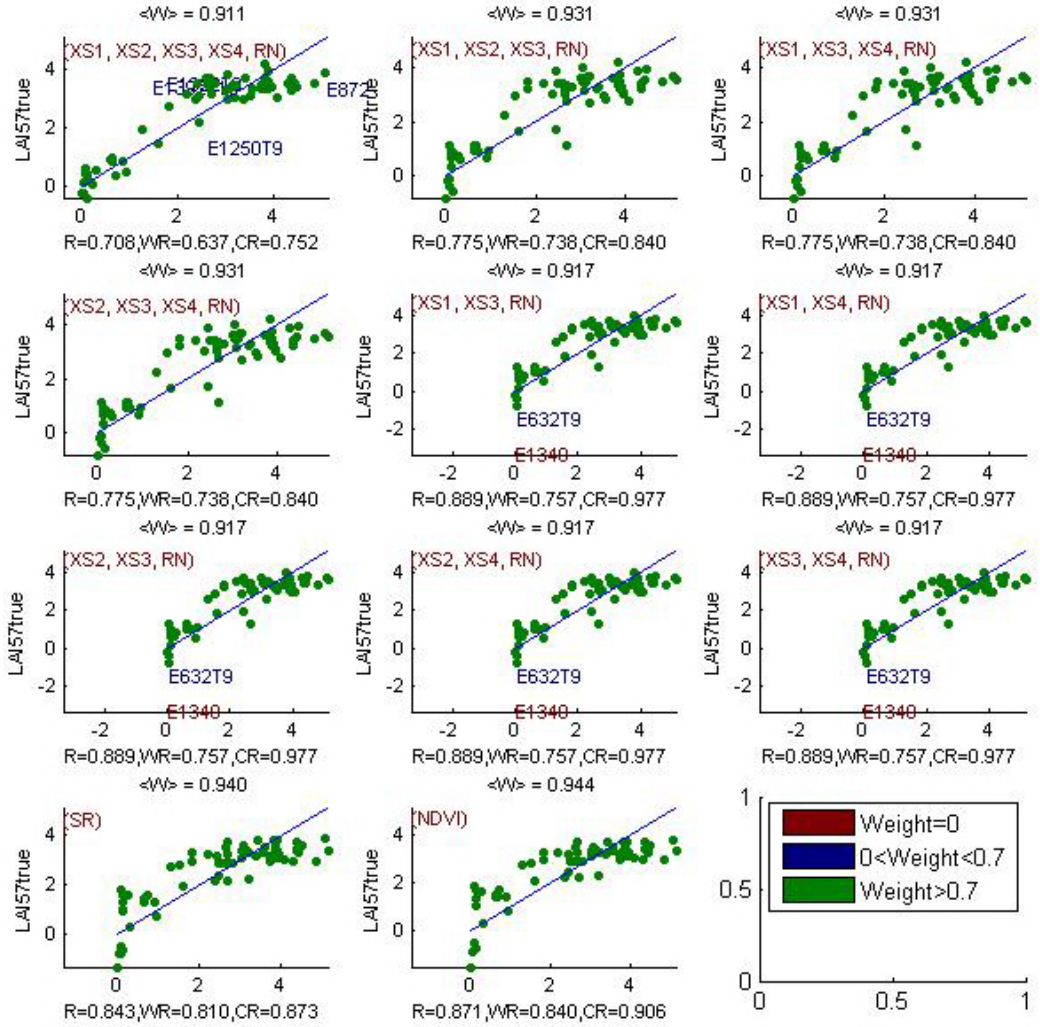

Figure 16. True Leaf Area Index at 57.5°: results for regression on reflectance using different band combinations. R is the root mean square error computed between LAI57true and estimated LAI57true. WR is the weighted root mean square error and CR is the cross validation root mean square error.

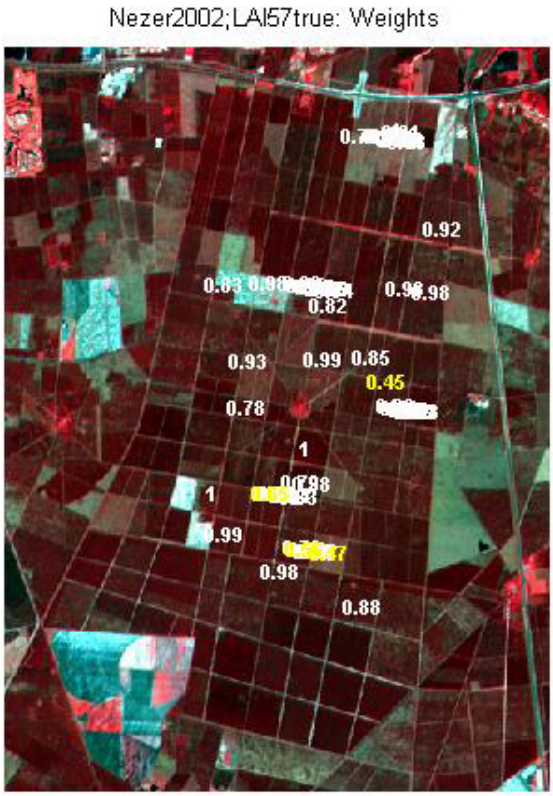

Figure 17. Weights associated to each ESU for the determination of LAI57true transfer function.

For the fCover, the XS1, XS2, XS3, XS4, RN (Figure 18 and Figure 19) combination on reflectance was selected since it provides the better results: lowest R, CR and WR values. Note that three weights are lower than 0.7.

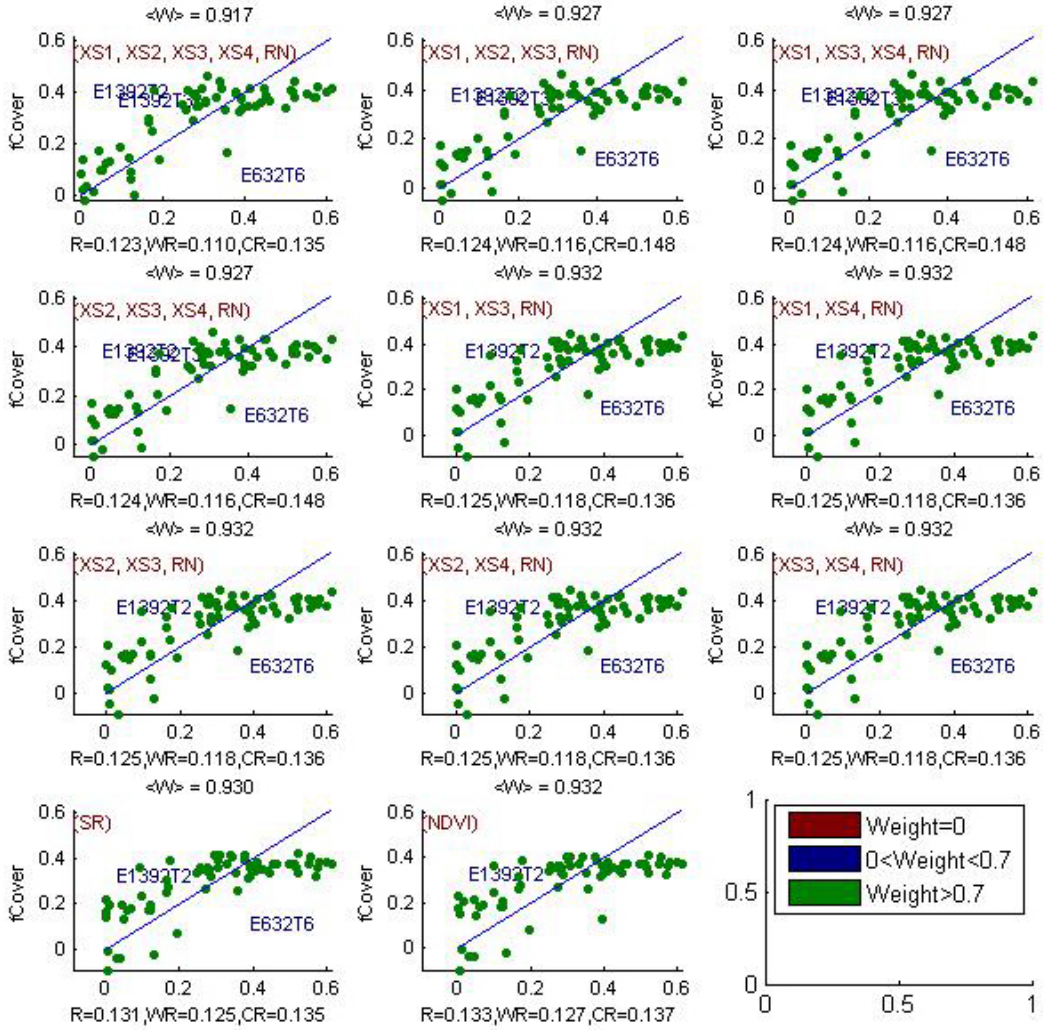

Figure 18. fCover: results for regression on reflectance using different band combinations. R is the root mean square error computed between fCover and estimated fCover. WR is the weighted root mean square error and CR is the cross validation root mean square error.

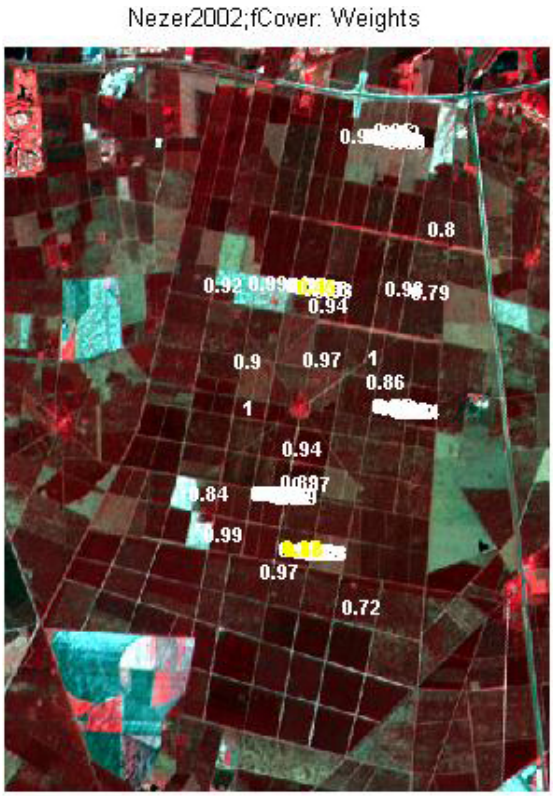

Figure 19. Weights associated to each ESU for the determination of fCover transfer function.

For the fAPAR, the XS2, XS3, XS4, RN (Figure 20 and Figure 21) combination on reflectance was selected since it provides a good compromise between the cross-validation RMSE, the weighted root mean square error and the number of weights lower than 0.7 (four). The following band combinations provide the same results: [XS1, XS2, XS3, RN]; [XS1, XS3, XS4, RN].

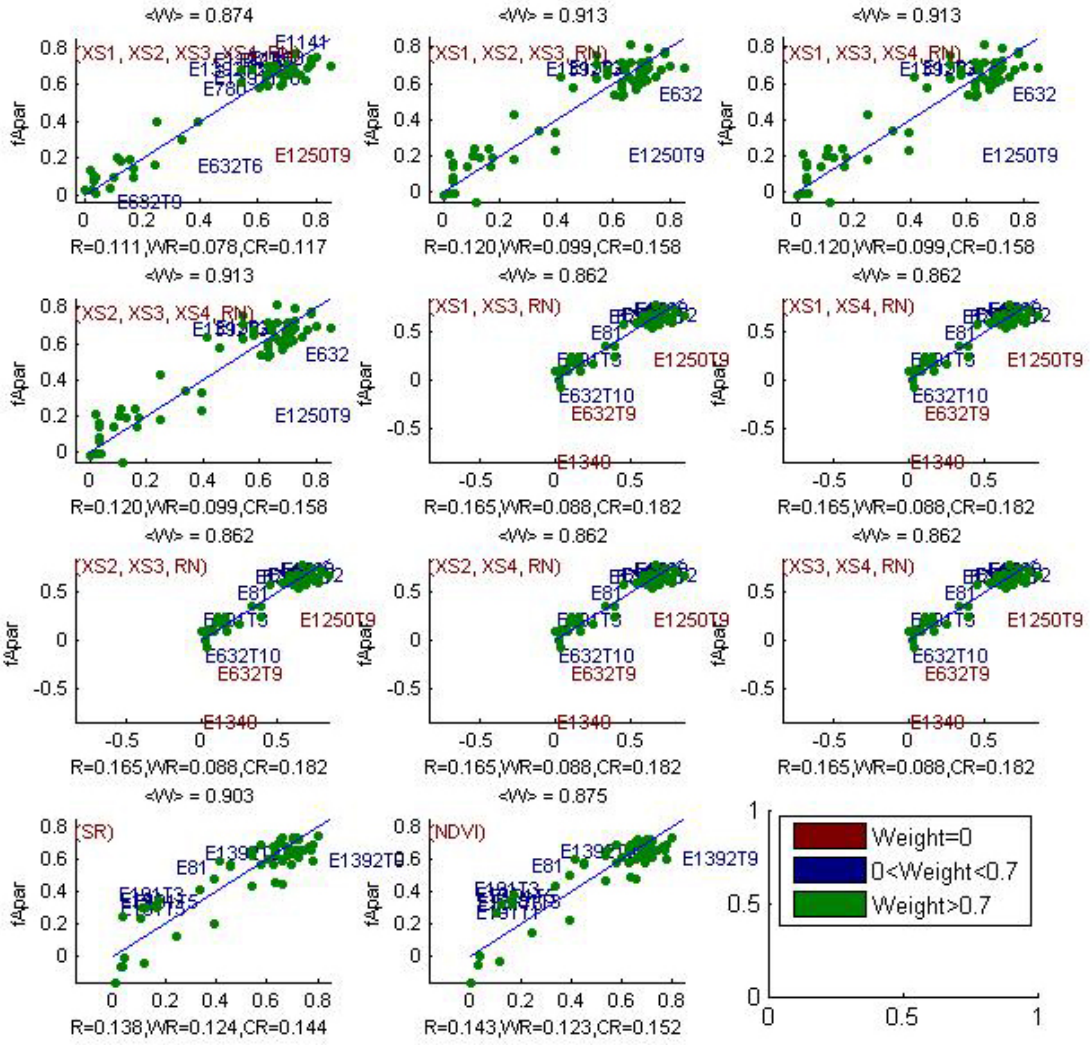

Figure 20. fAPAR: results for regression on reflectance using different band combinations. R is the root mean square error computed between fAPAR and estimated fAPAR. WR is the weighted root mean square error and CR is the cross validation root mean square error.

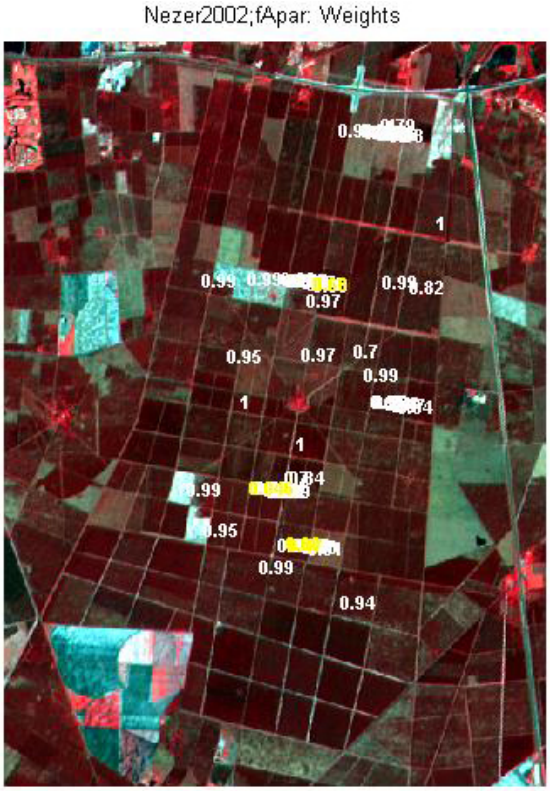

Figure 21. Weights associated to each ESU for the determination of fAPAR transfer function.

Note that E1250T9, E1392T2, E1392T3 and E1392T10 (pine stands) generally have a weight lower than 0.7 (E1250T9 and E1392T10 are close to paths). For LAI variables, the regression on reflectance using combinations with two bands (+RedNir) systematically excludes E1340 (young pine stand: only one vegetation stratum; green vegetation very sparse). Its weight is equal to zero.

Following, the results of the transfer function (Table 2):

Variable	Band Combination	RMSE	Weighted RMSE	Cross-valid RMSE
LAIeff	7.9695 + 58.589(XS2) - 118.98(XS3) - 38.424(XS4) + 293.84(RN)	0.462	0.387	0.490
LAItrue	4.2963 + 84.325(XS1) -70.437(XS2) - 9.3017(XS3) - 22.426(XS4) + 79.288(RN)	0.747	0.572	0.785
LAI57eff	3.5848 + 41.04(XS1) - 42.208(XS2) - 9.3074(XS3) - 13.515(XS4) + 83.497(RN)	0.413	0.363	0.438
LAI57true	4.7493 + 67.811(XS1) - 57.695(XS2) - 6.1521(XS3) - 25.448(XS4) + 84.23(RN)	0.708	0.637	0.752
fCover	-0.44873 + 26.144(XS1) - 14.714(XS2) + 1.1294(XS3) - 2.0372(XS4) - 21.965(RN)	0.123	0.110	0.135
fAPAR	2.5113 + 18.531(XS2) - 35.943(XS3) - 11.531(XS4) + 81.814(RN)	0.120	0.099	0.158

RN = Red*NIR

Table 2. Transfer function applied to the whole site for the different biophysical variables, and corresponding errors

3.3. Applying the transfer function to the Nezer SPOT image extraction

Figure 22 presents the biophysical variable maps obtained with the transfer function described in Table 2 for the classes 1, 2, 3, 4 and 5. The maps obtained for the six variables are consistent, showing similar patterns: low

LAIeff values where low fCover or fAPAR are observed and conversely… Note that one LAIeff pixel is higher than 14. However, its weight is insignificant on the scale to the Nezer site. The difference between effective LAI and true LAI is significant (see the average values in Figure 22). This was expected when looking the LAIeff/LAItrue relationship, showing that for high LAI the difference between the two can be significant.

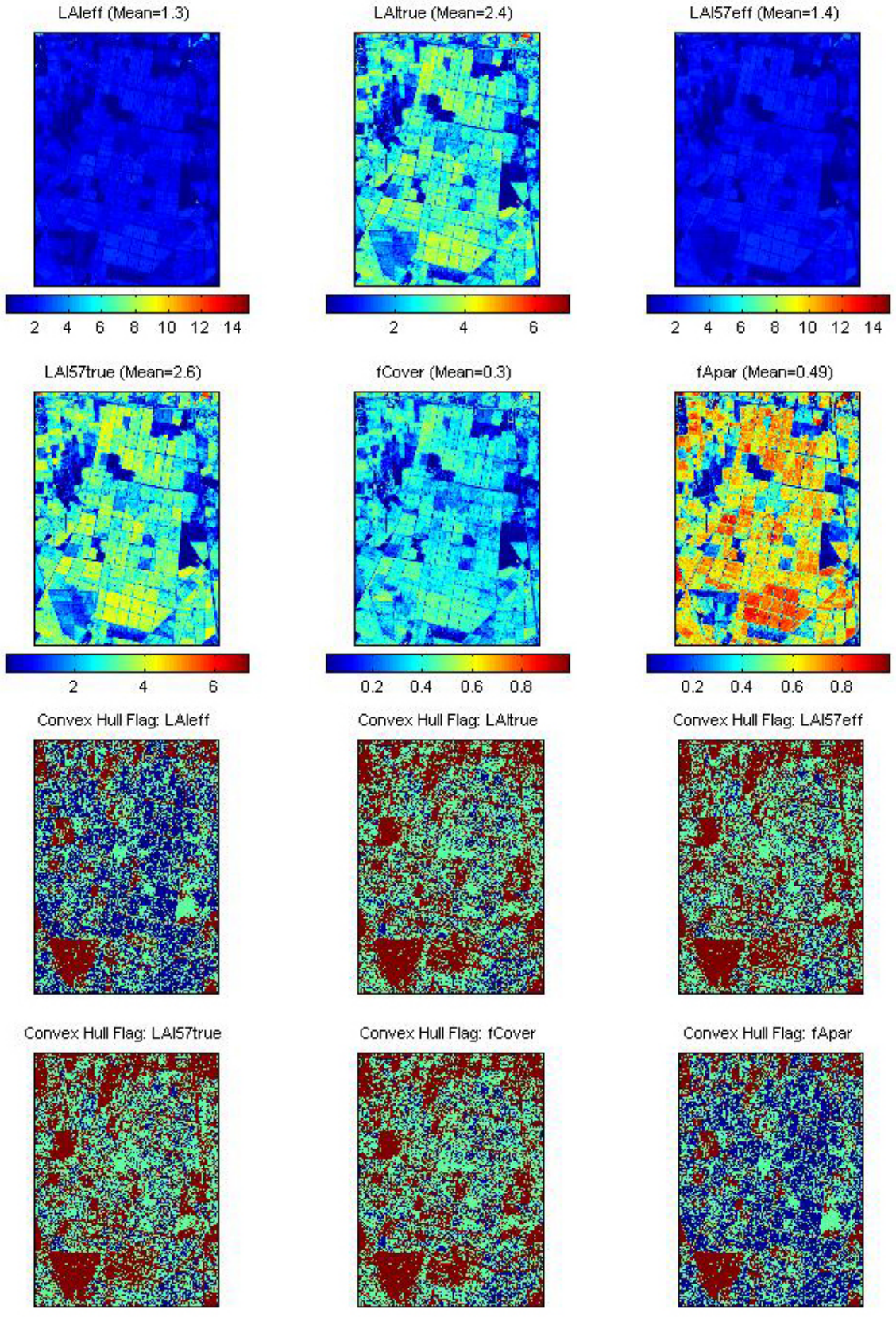

Figure 22. High resolution biophysical variable maps applied on the Nezer site (top). Associated Flags are shown at the bottom: blue and light blue correspond to the pixels belonging to the 'strict' and 'large' convex hulls, red to the pixels for which the transfer function is extrapolating.

The flag maps are comparable between LAItrue, LAI57eff, LAI57true, fCover and between LAIeff and fAPAR. The extrapolation mainly corresponds to bare soil, roads, paths, highest NVDI pixels (§2.3.2)… The pixels inside the strict convex hull for are more numerous in the LAIeff and fCover maps. This is due to the choice of the band combination.

4. Conclusion

The 'REG' method is applied to the classes 1, 2, 3, 4 and 5 by using 68 ESUs. The representativeness of the land cover of the different ESUs is good, even if classes are under-represented (bare soil, highest NDVI values are…, §2.3.2). The results of the robust regression are also satisfactory and the maps obtained for the biophysical variables are consistent. The flag associated to each map show that the extrapolation is mainly related to the problems of representativeness of the land cover and the band combination. For all the variables, the regression coefficients are computed by relating the variable itself to reflectance (§3.2.1).

The biophysical variable maps are available in France Zone III Sud (datum: Nouvelle Triangulation Française) and UTM, 30 North (datum: WGS-84) at 20 m resolution.

5. Acknowledgements

We want to thank: Gaston **Courrier**, Brice **Ferry**, Patrick **Moreau**, Sandra **Debesa**, Mickael **Pardé**, Jean-Marc **Bonnefond**, Didier **Garrigou** and Dominique **Guyon** (INRA, Bioclimatologie, Bordeaux) for the organisation and participation to the campaign.

ANNEX

Ground measurement acquisition report for the VALERI site **Nezer** (France)

sampled from 08/04/2002 to 25/04/2002

Dominique GUYON
Organization: INRA, Bioclimatologie, BORDEAUX, France
email: guyon@bordeaux.inra.fr

Date of report: 20 October 2002

People participating to the field experiment:

Firstname & Name	0rganization
Dominique GUYON	INRA, Bioclimatologie, Bordeaux (F)
Gaston COURRIER	INRA, Bioclimatologie, Bordeaux (F)
Brice FERRY	INRA, Bioclimatologie, Bordeaux (F)
Patrick MOREAU	INRA, Bioclimatologie, Bordeaux (F)
Sandra DEBESA	INRA, Bioclimatologie, Bordeaux (F)
Mickael PARDé	INRA, Bioclimatologie, Bordeaux (F)
Jean-Marc BONNEFOND	INRA, Bioclimatologie, Bordeaux (F)
Didier GARRIGOU	INRA, Bioclimatologie, Bordeaux (F)

Site coordinates

	Lat-Long WGS-84 (Deg min.00)		UTM / WGS-84 UTM		Other projection*	
	Lat.	Long.	Easting	Northing	Easting	Northing
Upper left corner	1°05.15'W	44°37.20'N			328000	3263000
Lower right corner	0°59.45'W	44°34.14'N			336000	3252000

*The other projection user is LAMBERT3. All the characteristics are provided in the following table (see http://www.avignon.inra.fr/valeri/, methodology page, GPS document for more information):

Geodesic Map Datum		Map Projection	
Associated Ellipsoïd	Clarke 1880	Latitude of origin	44°06'00"
Semi-major axe	6378249.2 m	Longitude of origin	2°20'14.025"
Semi-minor axe	6356515.0 m	Parallels 1st	43°11'57.449"
1/flattening		2nd	44°59'45.938"
Eccentricity		Xo: false easting	600000
		Yo: false northing	3200000
		Scale factor	0.99987750

Ground control points

# Name	Device	Month	Day	Hour	Minute	Easting(m)	Northing(m)
#							
GCP1	gpsYellow	4	23			333121	3261746
GCP2	gpsYellow	4	23			333509	3261673
GCP3	gpsYellow	4	23			334050	3260156
GCP4	gpsYellow	4	23			333533	3259541
GCP5	gpsYellow	4	23			333929	3259470
GCP6	gpsYellow	4	23			331686	3259415
GCP7	gpsYellow	4	23			332159	3259324
GCP8	gpsYellow	4	23			331024	3259312
GCP9	gpsYellow	4	23			332646	3259229
GCP10	gpsYellow	4	23			332108	3259097
GCP11	gpsYellow	4	23			331511	3258442
GCP12	gpsYellow	4	23			332482	3258276
GCP13	gpsYellow	4	23			332968	3258193
GCP14	gpsYellow	4	23			331397	3257859
GCP15	gpsYellow	4	23			332373	3257667
GCP16	gpsYellow	4	23			331332	3257577
GCP17	gpsYellow	4	23			333381	3257524
GCP18	gpsYellow	4	23			333902	3257429
GCP19	gpsYellow	4	23			332222	3256889
GCP20	gpsYellow	4	23			332147	3256392
GCP21	gpsYellow	4	23			330744	3256165
GCP22	gpsYellow	4	23			332047	3255907
GCP23	gpsYellow	4	23			330989	3255582
GCP24	gpsYellow	4	23			331959	3255406

*This is extracted from the Excel file GPSnezer2002.xls

GPS system used: Garmin 12 CX (ID= gpsYellow).
Typical uncertainty of GPS position: RMSE= 10.2 m for the GCPs displayed in the above table. These GCPs are situated at road crossings.

Description of the site and land cover

Category according to IGBP classification

Evergreen Needleleaf Forest (FORMLISTEDEROUL).

Comments on the land cover

The site is located in the Landes forest which covers about 1 million hectares in the South West of France and where maritime pine (*Pinus pinaster* Ait.) is the dominant species.

The study area is covered in major part by large and homogeneous (even-aged trees) stands of maritime pine which are intensively managed. The mean size of stands is about 500 x 500m. Their various stages of development range from the sowing to the clear-cutting, which is performed mostly after 50 years. The remainder consists mainly of small deciduous wood lands, mosaics of small-sized stands of deciduous species or pine, large agricultural fields, urban and industrial areas, and unmanaged heath lands (see the land use map in figure 1).

In 2002 the experiment was focused in the central part of the study area. This part covers roughly 5*8 km. It is made up mainly of stands of pine and several rare small islands of deciduous trees.

Topography

The ground surface is nearly flat. The average altitude is close to 25 meters.

Land cover map

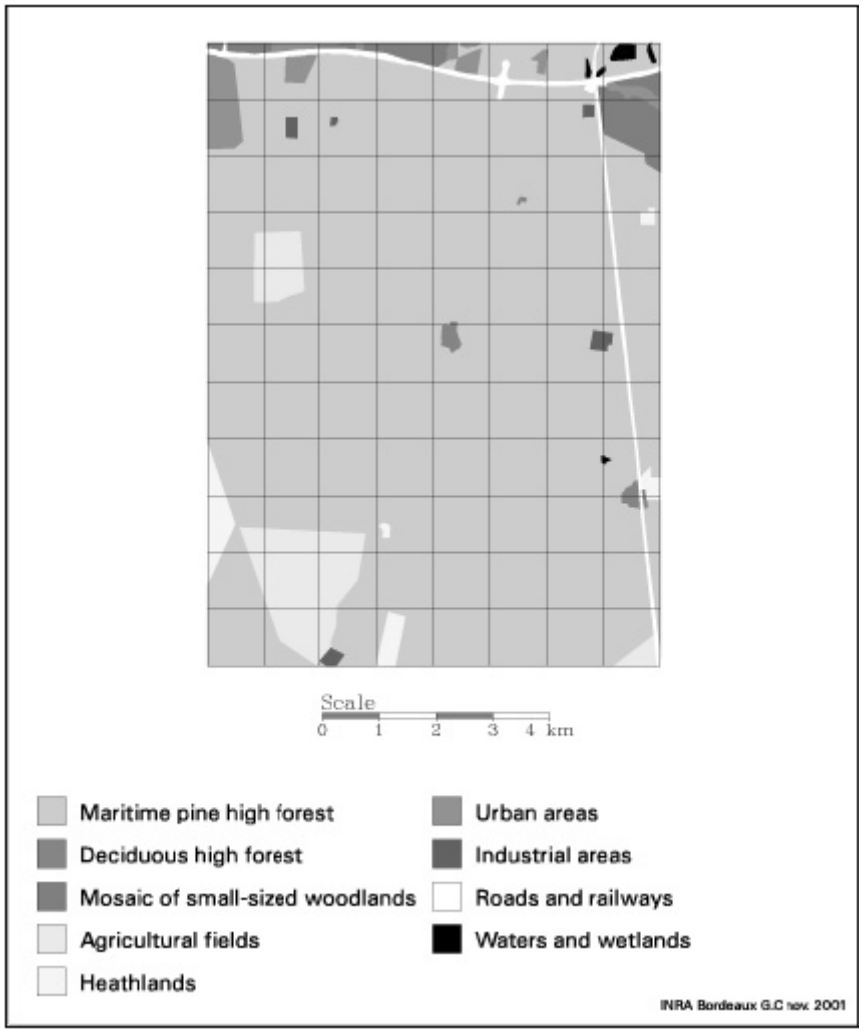

Figure 1: Land use map in 2000 (from aerial photographs and Spot images)

Spatial Sampling scheme

Sensors used for sampling the ESUs

	Method	Comments
☒	Hemispherical photographs	• Instrument : NIKON COOLPIX995 (Serial number : 4512539) + fisheye converter FC-E8 • Data compression: none for photographs towards the sky (format TIFF), else JPEG compression • Geometrical resolution: maximal; image size= 1536*2048 pixels • Recording in colour • Measurement below the tree storey: sensor height=0.8 to 1.3m (CP measurements) • Measurement below the undergrowth: at ground level. Performed when green vegetation is not sparse and >20cm (CS measurements) • Else shooting towards the ground (CSB measurements) • Illumination conditions: various sky conditions at any time of the day, except for high solar elevation (about >50°) when the sky is clear • Measured ESUs: all
☒	LAI2000	• ID and Serial number of instruments: VAL1= PCH-0979, VAL3= PCH-1467, VAL4=PCH-1544 • Measurement under the tree storey: height=0.8 to 1.3m; 3 repetitions on each point; without view cap both below and above the canopy (CP measurements) • Measurement under the undergrowth: at ground level; without view cap above the canopy; with view cap of 180° below the canopy; gap fraction measured in two opposite directions on each point, with 3 repetition (CS measurements) • Illumination conditions: clear sky, solar elevation <16°, at evening • Measured ESUs: all except those distributed along the transects
☐	TRAC	
☐	Ceptometer	
☐	Direct measurements	
☐	Other	

Sampling strategy for the ESU

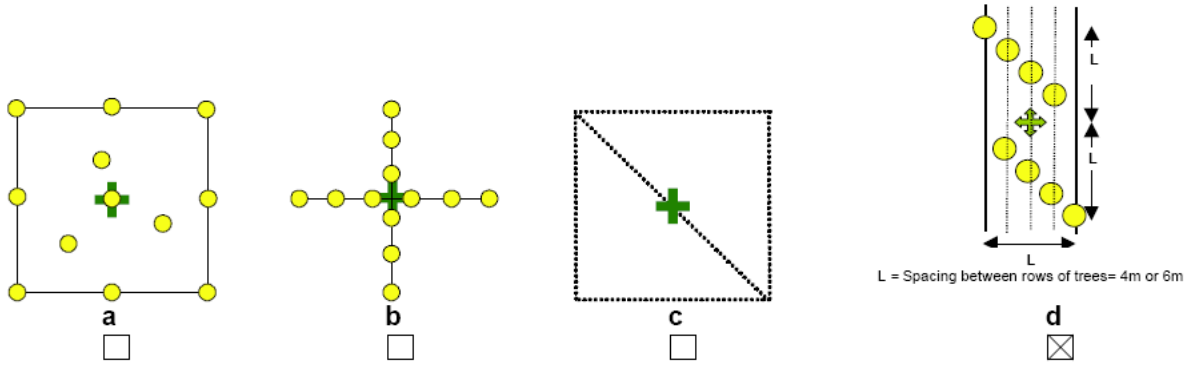

☐ ☐ ☐ ☒

Distribution of the Elementary sampling units

Strategy used to define the location of the ESUs:
• According to the distribution of the age classes of pine stands
• Accessibility
• Local variability: sampling within several stands with ESUs separated by 50 meters (+ in figure 2). They constituted five 500m transects

• Spatial variability at larger scale: sampling of the variability between stands with ESUs whose spacing ranges from 100-500 meters to several kilometres (* in figure 2).

Figure 2: Spatial distribution of the ESUs

* Sampling of the variability between stands
+ Sampling within stands (transects)
The 1km²-grid gives the scale.
In background : SPOT4 image acquired on the 21th April 2002.

Method used for locating the ESUs

We did not use GPS system for locating the ESUs because of difficulties to receive signal beneath the tree canopy. The geographical location of the centre of each ESU was provided from ground measurement of its distance to landmarks referenced in a geographic database of INRA.

The mean error of position of the landmarks equals 16.7 m. But the relative accuracy is better because of a systematic shift of roughly 10 meters towards North-West.

List of the ESUs

ESUs measurements (source: GPSnezer2002.xls)
Names begining with a number correspond to ESUs ID
columns 2-6 : locating
method for locating: gpsYellow (by using GPS = GARMIN12CX) , noGPS (by measuring distance to landmarks)
columns 7-11 : LAI measurements at ground
date of LAI measurements with hemispherical photographs: hp-CP= tree layer, hp-CS= trees+undergrowth, hp-CSB= undergrowth (towards ground);
date of LAI measurements with LAI2000 sensors: L-CP=tree layer, L-CS = trees+undergrowth
format : DD/MM/YY
column 12 : comments

# Name	Easting (m)	Northing (m)	hp-CP	hp-CS	hp-CSB	L-CP	L-CS	Comments on the vegetation status, condition of acquisitions, etc...
# 1	5	6	7	8	9	10	11	12
72000	333468	3261754		08/04/2002	22/04/2002		22/04/2002	young pine stand: only one vegetation stratum (trees + undergrowth)
81000	333584	3261734		08/04/2002	22/04/2002		19/04/2002	young pine stand: only one vegetation stratum (trees + undergrowth)
162000	332973	3261671	08/04/2002	08/04/2002	22/04/2002	24/04/2002	24/04/2002	pine stand
181000	333449	3261644		22/04/2002	22/04/2002		22/04/2002	young pine stand: only one vegetation stratum (trees + undergrowth)
191000	333564	3261619		08/04/2002	22/04/2002		19/04/2002	young pine stand: only one vegetation stratum (trees + undergrowth)
391000	334201	3260306	18/04/2002	18/04/2002	22/04/2002	22/04/2002	22/04/2002	pine stand
582000	331641	3259477			09/04/2002			young pine stand: only one vegetation stratum (trees + undergrowth); low cover fraction (almost bare soil)
590000	330949	3259453	18/04/2002	18/04/2002	22/04/2002	22/04/2002	22/04/2002	pine stand
632000	332534	3259396	08/04/2002		22/04/2002	18/04/2002		pine stand; green vegetation of understorey very sparse and <20cm
642000	332492	3259155	08/04/2002	08/04/2002	22/04/2002	18/04/2002		pine stand; green vegetation of understorey sparse and <20cm
671000	333629	3259420	09/04/2002		22/04/2002	18/04/2002		pine stand; no green vegetation in understorey
681000	334023	3259345	09/04/2002	09/04/2002	22/04/2002	18/04/2002	18/04/2002	pine stand
760000	332428	3258364	18/04/2002	22/04/2002	22/04/2002	18/04/2002		young pine stand; dried vegetation is very abundant in understorey
780000	333133	3258392	09/04/2002	09/04/2002	22/04/2002	22/04/2002	22/04/2002	pine stand
830000	331322	3258319	18/04/2002	18/04/2002	22/04/2002	24/04/2002	24/04/2002	pine stand
872000	333357	3258030	10/04/2002	10/04/2002	22/04/2002	22/04/2002		pine stand ; dried vegetation is very abundant in understorey
882000	333797	3257596	10/04/2002	10/04/2002	22/04/2002	24/04/2002	24/04/2002	pine stand
940000	331293	3257647	18/04/2002	18/04/2002	22/04/2002	22/04/2002	22/04/2002	pine stand
1042000	332127	3257035	18/04/2002		22/04/2002	24/04/2002		pine stand; dried vegetation is very abundant in understorey
1130000	332101	3256543	10/04/2002	22/04/2002	22/04/2002	19/04/2002	19/04/2002	pine stand
1141000	332220	3256524	10/04/2002	22/04/2002	22/04/2002	19/04/2002	19/04/2002	pine stand
1200000	330728	3256354			09/04/2002			young pine stand: only one vegetation stratum (trees + undergrowth); low cover fraction (almost bare soil)
1250000	332002	3256323	10/04/2002	10/04/2002	22/04/2002	19/04/2002	19/04/2002	pine stand
1340000	330967	3255760			09/04/2002		24/04/2002	young pine stand: only one vegetation stratum (trees + undergrowth); green vegetation very sparse and <20cm
1392000	332256	3255527	10/04/2002	10/04/2002	22/04/2002	19/04/2002	19/04/2002	pine stand
1450000	331798	3255191	18/04/2002	18/04/2002				pine stand
1480000	332993	3254682	18/04/2002	18/04/2002				pine stand
181001	333498	3261635		12/04/2002				young pine stand: only one vegetation stratum (trees + undergrowth)
181003	333400	3261653		12/04/2002				young pine stand: only one vegetation stratum (trees + undergrowth)
181004	333351	3261662		12/04/2002				young pine stand: only one vegetation stratum (trees + undergrowth)
181005	333302	3261671		12/04/2002				young pine stand: only one vegetation stratum (trees + undergrowth)
191001	333515	3261628		12/04/2002				young pine stand: only one vegetation stratum (trees + undergrowth)
191003	333613	3261610		12/04/2002				young pine stand: only one vegetation stratum (trees + undergrowth)
191004	333662	3261601		12/04/2002				young pine stand: only one vegetation stratum (trees + undergrowth)
191005	333711	3261592		12/04/2002				young pine stand: only one vegetation stratum (trees + undergrowth)
632001	332583	3259387	12/04/2002		12/04/2002			pine stand; green vegetation of understorey sparse and <20cm
632003	332485	3259405	12/04/2002	12/04/2002				pine stand
632004	332436	3259414	12/04/2002	12/04/2002				pine stand
632005	332387	3259423	12/04/2002	12/04/2002				pine stand
632006	332337	3259433	12/04/2002		12/04/2002			low trees density ; green vegetation of understorey sparse and <20cm
632007	332288	3259442	12/04/2002		12/04/2002			low trees density ; green vegetation of understorey sparse and <20cm
632008	332239	3259451			12/04/2002			clear cut; green vegetation = sparse and <20cm
632009	332193	3259460			12/04/2002			clear cut; green vegetation = sparse and <20cm
632010	332141	3259469			12/04/2002			young pine stand: only one vegetation stratum (trees + undergrowth); green vegetation very sparse and <20cm
882001	333847	3257587	15/04/2002	15/04/2002				pine stand
882003	333747	3257605	15/04/2002	15/04/2002				pine stand
882004	333697	3257614	15/04/2002	15/04/2002				pine stand
882005	333647	3257623	15/04/2002	15/04/2002				pine stand
882007	333547	3257642	15/04/2002	15/04/2002				pine stand
882008	333497	3257651	15/04/2002	15/04/2002				pine stand
882009	333447	3257660	15/04/2002	15/04/2002				pine stand
1250001	332052	3256314	16/04/2002	16/04/2002				pine stand
1250003	331952	3256332	16/04/2002	16/04/2002				pine stand
1250004	331902	3256341	16/04/2002	16/04/2002				pine stand
1250005	331852	3256350	16/04/2002	16/04/2002				pine stand
1250006	331802	3256360	16/04/2002	16/04/2002				pine stand
1250007	331752	3256369	16/04/2002	16/04/2002				pine stand
1250008	331702	3256378	16/04/2002	16/04/2002				pine stand
1250009	331652	3256387	16/04/2002	16/04/2002				pine stand
1392001	332056	3255564	15/04/2002	15/04/2002				pine stand
1392002	332106	3255554	15/04/2002	15/04/2002				pine stand
1392003	332156	3255545	15/04/2002	15/04/2002				pine stand
1392004	332206	3255536	15/04/2002	15/04/2002				pine stand
1392006	332306	3255518	15/04/2002	15/04/2002				pine stand
1392007	332356	3255509	15/04/2002	15/04/2002				pine stand
1392008	332406	3255500	15/04/2002	15/04/2002				pine stand
1392009	332456	3255490	15/04/2002	15/04/2002				pine stand
1392010	332505	3255481	15/04/2002	15/04/2002				pine stand

This is extracted from the Excel file GPSnezer2000.xls

The high spatial resolution image

Satellite

Satellite used: SPOT4 HRVIR2.
Level of processing: SPOTVIEW Basic 2B.
Projection type: LAMBERT III.
Date: 21 April 2002

Airborne

Describe the sensor and data with attention on radiometric calibration, atmospheric correction, and projection: *Not used.*

Atmosphere properties

For atmospheric correction of remote sensing data, aerosol optical depth and water vapour content were provided by AERONET network from measurements with the automatic sun photometer located in the INRA Research Centre of Bordeaux (N44°47', W00°34'), at about 40 km from the Nezer site.

Global and diffuse incoming radiation were measured in the NEZER site for assessing horizontal variations of atmosphere properties. An integrated sensor of photosynthetic active radiation (BF2, Delta-T Devices Ltd, Serial Number=) was used. It was set in the northern part of NEZER (333350m Easting, 3261750m Northing, Lambert3). Measurements were recorded from 29 March to 21 April 2002. The sampling frequency was equal to 1 minute.

Photo gallery

The photos illustrating the campaign are to be stored in the directory "photo gallery" and the labels should be indicated in the table above:

#	File name	Comments	date
1	ph1_sangliers1.JPG	The team number 2	2002-04-18 12:55
2	ph2_lai2000_CP.JPG	measurement below the tree storey with LAI2000	2002-04-19 18:34
3	ph3_hemisphericalphoto_CP.JPG	measurement below the tree storey with fish eye camera	2002-04-15 08:04
4	ph4_hemisphericalphoto_CP.JPG	measurement below the tree storey with fish eye camera	2002-04-15 10:10
5	ph5_hemisphericalphoto_CS.JPG	measurement below the undergrowth with fish eye camera	2002-04-15 07:54
6	ph6_hemisphericalphoto_CS.JPG	measurement below the undergrowth with fish eye camera	2002-04-15 14:57
7	ph7_hemisphericalphoto_CSB.JPG	measurement with fish eye camera towards the ground	2002-04-12 17:35